2012-04

Structural and dynamic characterization of Li12Si7 and Li12Ge7 using solid state NMR

Solid State Nuclear Magnetic Resonance,London : Academic Press,v. 42, p. 17-25, Apr. 2012
http://www.producao.usp.br/handle/BDPI/49949

Solid State Nuclear Magnetic Resonance 42 (2012) 17–25

Contents lists available at SciVerse ScienceDirect

Solid State Nuclear Magnetic Resonance

journal homepage: www.elsevier.com/locate/ssnmr

Structural and dynamic characterization of $Li_{12}Si_7$ and $Li_{12}Ge_7$ using solid state NMR

Sven Dupke [a], Thorsten Langer [b], Rainer Pöttgen [b], Martin Winter [a], Hellmut Eckert [a,*]

[a] Institute of Physical Chemistry, WWU Münster, Corrensstrasse 28/30, 48149 Münster, Germany
[b] Institute of Inorganic and Analytical Chemistry, WWU Münster, Corrensstrasse 28/30, 48149 Münster, Germany

ARTICLE INFO

Available online 24 September 2011

Keywords:
Lithium tetrelides
Solid state NMR
Structural characterization

ABSTRACT

Local environments and lithium ion dynamics in the binary lithium silicide $Li_{12}Si_7$, and the analogous germanium compound have been characterized by detailed ^6Li, ^7Li, and ^{29}Si variable temperature static and magic-angle spinning (MAS) NMR experiments. In the MAS-NMR spectra, individual lithium sites are generally well-resolved at temperatures below 200 K, whereas at higher temperatures partial site averaging is observed on the kHz timescale. The observed lithium chemical shift ranges of up to 60 ppm indicate a significant amount of electronic charge stored on the lithium species, consistent with the expectation of the extended Zintl–Klemm–Bussmann concept used for the theoretical description of lithium silicides. Furthermore the strongly diamagnetic chemical shifts observed for the lithium ions situated directly above the five-membered Si_5 rings suggest the possibility of aromatic ring currents in these structural elements. This assignment is confirmed further by $^{29}Si\{^7Li\}$ CPMAS-heteronuclear correlation experiments. The ^{29}Si MAS-NMR spectra of $Li_{12}Si_7$, aided by 2-D J-resolved spectroscopy, are well suited for differentiating between the individual sites within the silicon framework, while further detailed connectivity information is available on the basis of 2-D INADEQUATE and radio frequency driven recoupling (RFDR) spectra. Variable temperature static ^7Li NMR spectra reveal the onset of strong motional narrowing effects, illustrating high lithium ionic mobilities in both of these compounds.

1. Introduction

Due to the possible application of nano-silicon as a high capacity anode material in lithium ion batteries, lithium silicides, and the lithiation of silicon have attracted a lot of interest recently. The crystalline lithium silicides available through thermal synthesis routes are $Li_{12}Si_7$, Li_7Si_3, $Li_{13}Si_4$, and $Li_{21}Si_5$ [1–8]. Electrochemical lithiation of silicon so far has only resulted in amorphous Li_xSi material [9], and solid state NMR studies have been interpreted in terms of local lithium environments comparable to those present in crystalline silicides, their quantitative distribution depending on the extent of the electrochemical charge transfer executed [10–12]. Those results illustrate the prominent role of the metastable phase, $Li_{15}Si_4$ in particular; consistent with earlier results obtained by Obrovac and Christensen [13] and Hatchard and Dahn [14]. A major step in the understanding of silicon based anodes was achieved through the in-situ NMR study of the lithiation of silicon [10]. The ^7Li resonances of the known crystalline lithium silicides have distinguishable NMR shifts and can thus be utilized to determine the composition of the anode material by post mortem as well as in situ characterization. While these previous works provided a detailed understanding of the electrochemical lithiation process, both the static and magic-angle spinning NMR spectra measured at room temperature are strongly influenced by the lithium ion dynamics, resulting in partial or complete motional averaging of the NMR signals of crystallographically distinguishable lithium sites. In the lowest-lithium containing binary phase, $Li_{12}Si_7$, the detailed motional dynamics have been recently characterized by ^7Li relaxometry, leading to the identification and quantitative characterization of a very fast one-dimensional diffusion process and two additional three-dimensional diffusion processes, which are somewhat slower [15]. These motional processes need yet to be related to crystallographic information. In addition to an improved description of the motional processes in this compound, the electronic structure and bonding situation is of interest. Following the description given in Ref. [1], the structures of all the lithium silicides can be viewed in terms of an extended Zintl–Klemm–Busmann concept, where the excess electrons occupy cage orbitals formed by Li-2s states, surrounding the silicon structural elements in the framework. In $Li_{12}Si_7$ the chief structural elements are five-membered Si_5 rings, charge compensated by six lithium atoms (Li_6Si_5 units) and Y-shaped $Si(Si)_3$ stars, charge compensated by 12 lithium ions ($Li_{12}Si_4$ units),

* Corresponding author.
E-mail address: eckerth@uni-muenster.de (H. Eckert).

0926-2040/$ - see front matter © 2011 Elsevier Inc. All rights reserved.
doi:10.1016/j.ssnmr.2011.09.002

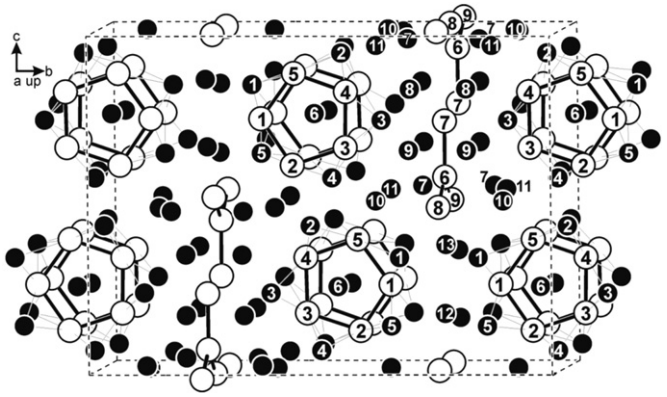

Fig. 1. Schematic depiction of the crystal structure of $Li_{12}Si_7$, indicating the various crystallographically distinct lithium and silicon sites.

respectively, occurring in a 2:1 ratio [8], see Fig. 1. The excess 2s electron density has been attributed to lithium species that are part of the $Li_{12}Si_4$ units. Subsequent theoretical studies have suggested various different modifications of this picture [16–19]. In order to gain deeper insights into the structure and bonding in $Li_{12}Si_7$, the present study reports a comprehensive solid state NMR characterization of the silicide framework using ^{29}Si MAS-NMR, aided by 2-D J-resolved, radio frequency driven recoupling (RFDR) and {^{7}Li}^{29}Si cross-polarization-heteronuclear correlation experiments. Furthermore, the bonding states of the various lithium ions and their differential dynamics in $Li_{12}Si_7$ and its analogous germanide phase are investigated by temperature dependent ^{6}Li MAS-NMR and ^{7}Li wideline NMR spectra.

2. Materials and methods

2.1. Synthesis

Starting materials for the preparation of $Li_{12}Si_7$ and $Li_{12}Ge_7$ were lithium rods (Merck, >99%), silicon lumps (Wacker, >99.9%), and germanium lumps (Sigma Aldrich, >99.9%), respectively. Synthesis of the ^{29}Si enriched $Li_{12}Si_7$ sample was carried out using silicon powder (99.34% ^{29}Si, STB Isotope Germany). The lithium rods were cut into smaller pieces under dry paraffin oil and subsequently washed with *n*-hexane. The lithium pieces were kept in Schlenk tubes under argon prior to reaction. Argon was purified with titanium sponge (900 K), silica gel, and molecular sieves. The lithium pieces were mixed with the silicon and germanium, respectively, in the ideal 12:7 atomic ratio under flowing argon and then arc-welded in a tantalum tube under an argon pressure of about 100 mbar. The tantalum tubes were then placed in a water-cooled sample chamber of an induction furnace. The samples were rapidly heated to 1100 K and held at that temperature for 10 min. Subsequently, the samples were rapidly cooled to 900 K and annealed at that temperature for 2 h before they were quenched by switching off the power supply. The brittle products could be easily removed from the tantalum tube, no reaction with the container material was observed. Both products exhibit as prepared metallic luster while ground powders are gray. Since $Li_{12}Si_7$ and $Li_{12}Ge_7$ are not stable in air they were kept in argon-filled Schlenk tubes.

2.2. X-ray powder diffraction

The $Li_{12}Si_7$ and $Li_{12}Ge_7$ samples were characterized through Guinier powder patterns using Cu Kα_1 radiation and α-quartz (a=491.30 and c=540.46 pm) as an internal standard. The Guinier camera was equipped with an imaging plate technique (Fujifilm, BAS-READER 1800). The lattice parameters were obtained through a least-squares fitting routine. The correct indexing was ensured through comparison of the experimental pattern with a calculated one. All prepared samples are crystalline and pure within the detection limit of x-ray diffraction and have an orthorhombic unit cell (space group *Pnma*). The refined lattice parameters for $Li_{12}Si_7$ (a=860.0(1), b=1976.7(3), c=1434.0(3) pm) and $Li_{12}Ge_7$ (a=871.8(3), b=2005.1(8), c=1454.0(6) pm), are in good agreement with the data reported in the literature.

2.3. Solid state NMR

$^{6/7}$Li and ^{29}Si MAS-NMR studies were carried out on a Bruker Avance DSX spectrometer working at 9.4 T using a commercial 4 mm Bruker VT MAS triple resonance probe. All samples were powdered and diluted with dried boron nitride in a 1:1 mass ratio to minimize undesirable probe detuning or sample heating effects due to the metallic character of the samples. ^{29}Si enriched samples were used for all ^{29}Si and double resonance experiments, while $^{6/7}$Li NMR was done on samples in natural abundance. The MAS-NMR spectra for all nuclei were obtained from Bloch decays following a single 90° pulse. A typical 90° pulse length was 4 μs and typical delays for ^{7}Li 10 s, for ^{6}Li 120–300 s, for ^{29}Si 10 s. Dry nitrogen gas was used for MAS experiments with typical spinning speeds of 10 kHz for room temperature and 5–8 kHz for low-temperature MAS. Temperatures were calibrated using the ^{207}Pb resonance of lead nitrate as previously described [20,21]. Deconvolution of the spectra was done using the DMfit software [22]. A 1 M LiCl solution and tetramethyl silane (TMS) were used as references for $^{6/7}$Li and ^{29}Si, respectively. Two-dimensional (2-D) ^{29}Si J-resolved spectra were acquired with a z-filtered echo sequence following a 15*(90°)-saturation comb on the ^{29}Si enriched sample with 256 transients recorded with a recycle delay of 2 s and 384 steps at an increment of 200 μs. 2-D INADEQUATE spectra were measured using a standard sequence with phase cycling according to reference [23]. 112 experiments with 256 scans and a 5 s recycle delay were acquired with an increment of 20 μs and an echo time corresponding to 1.9 ms. Even though this value is smaller than the theoretically calculated ideal echo time 1/4 J=4.0 ms, this timing turned out to be more effective for suppressing cross-peaks arising from relayed coupling effects. Radio frequency dipolar recoupling (RFDR) studies [24] were carried out at 7.0 T, using a spinning speed of 10 kHz with a mixing time of 800 μs and an increment of 25 μs, which resulted in 8 applied π pulses in each experiment that are phase-cycled according to the XYXY YXYX scheme. The signal was detected after a rotor-synchronized echo with an echo-time of one rotor period. 16 transients were collected for the direct dimension and 384 increments in the indirect dimension using the STATES-TPPI method for quadrature detection in the F1 dimension and a recycle delay of 10 s. ^{29}Si{^{7}Li} cross-polarization and 2-D heteronuclear correlation experiments were conducted at a common nutation frequency of 33.3 kHz, using a ramp for the ^{7}Li radiofrequency power, a recycle delay of 5 s and a contact time of 5 ms. For the 2-D heteronuclear correlation experiment 64 transients and 256 increments of 60 μs were recorded. Static ^{7}Li NMR was conducted on a Bruker Avance DSX spectrometer working at 4.7 T with a commercial static 5 mm Bruker VT probe for measurements above RT and a home-built static 5 mm probe below room temperature. A standard 90°–τ–180°–τ–acquire pulse sequence emphasizing the central transition was applied.

3. Results and interpretation

3.1. ^{29}Si MAS and $^{29}Si\{^{7}Li\}$ CPMAS NMR

Fig. 2 shows the ^{29}Si MAS-NMR spectrum of a ^{29}Si enriched sample of $Li_{12}Si_7$, obtained both in the single pulse mode and via cross-polarization from ^{7}Li. In the single-pulse mode, all the nine crystallographically distinct Si sites are resolved into separate resonances. The relative peak areas, taking into account the contributions of the spinning sidebands, are consistent with the ring-to-star ratio of 2:1 present in the crystal structure. The additional peak at 351 ppm was found to be absent in the ^{29}Si MAS spectrum of the natural abundance sample (data not shown) and is attributed to an unknown impurity. Interestingly, two of the constituent Si atoms of the five-membered silicon ring are spectrally rather close to each other (near 300 ppm), whereas three resonances occur in a different chemical shift region (around 170–230 ppm). A similar situation obtains for the terminal silicon atoms of the Si_4 star unit, which are separated by more than 100 ppm. The connectivity within the Si_5-ring can be confirmed by further experimentation using 2-D NMR methods. Figs. 3 and 4 show INADEQUATE and RFDR results, exposing the direct connectivities within the Si_5 rings. In both experiments, the attainable signal-to-noise ratios were too low for allowing connectivities within the Si_4 star to be detected. However, the J-resolved spectrum, shown in Fig. 5, is able to reveal the multiplicities of each of the ^{29}Si resonances of $Li_{12}Si_7$. Inspection of the individual slices in the 2D spectrum yields coupling constants of 82 Hz for the doublets (outer Si of the star), 74 Hz for the quartet (inner Si atom of the star), and 62 Hz for the triplets (ring). These values are comparable to those found in cyclic organic systems [25]. Table 1 gives a summary of all the NMR observables measured for the silicon atoms contained in the two structural moieties present. As the coupling constants extracted for the doublets and the quartet should actually be identical, the experimentally observed values (82 vs. 74 Hz) must be considered to be identical within the experimental error.

Fig. 2 also shows $^{29}Si\{^{7}Li\}$ CPMAS-NMR spectra at room temperature and at 200 K. While in the room temperature spectrum all the resonances of the Si_5 ring are easily detectable, only one of the three terminal silicon sites belonging to the Si_4 star unit is observable (marked by an arrow in Fig. 2a). Numerous variations of either the ^{29}Si resonance offset, the spinning frequency (5–10 kHz) or the contact time (3–10 ms) gave identical results. They indicate that the central Si atom and two of the three terminal end groups of the Si_4 star unit are surrounded only by lithium ions of extremely high mobility, such that no cross-polarization can take place at room temperature. Fig. 2b shows that the situation is different at 200 K. All of the ^{29}Si resonances are easily observed, as the lithium ionic motion has slowed down sufficiently to enable cross-relaxation via heteronuclear ^{7}Li–^{29}Si dipole–dipole interactions.

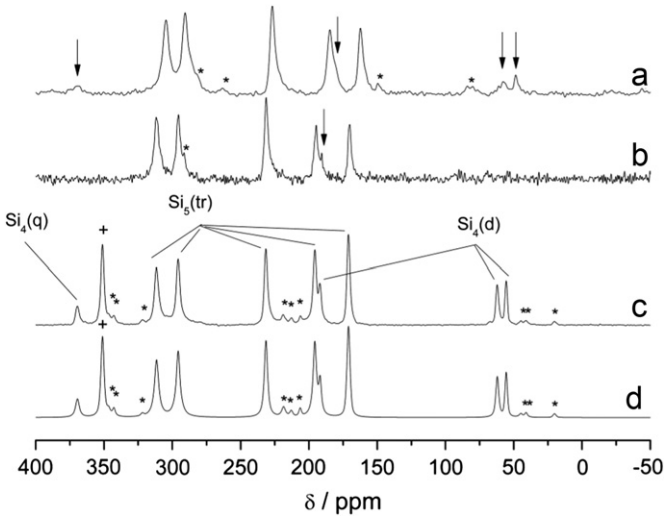

Fig. 2. $\{^{7}Li\}^{29}Si$ CPMAS-NMR spectrum of $Li_{12}Si_7$ at 200 K (a) and at room temperature (b), comparison with the single-pulse spectrum (c), and its simulation (d). Peak multiplicities as obtained from J-resolved experiments are indicated as d (doublet), tr (triplet), q (quartet). Arrows in (a) and (b) indicate signals attributed to the Si_4 star units. Spinning sidebands are marked by asterisks.

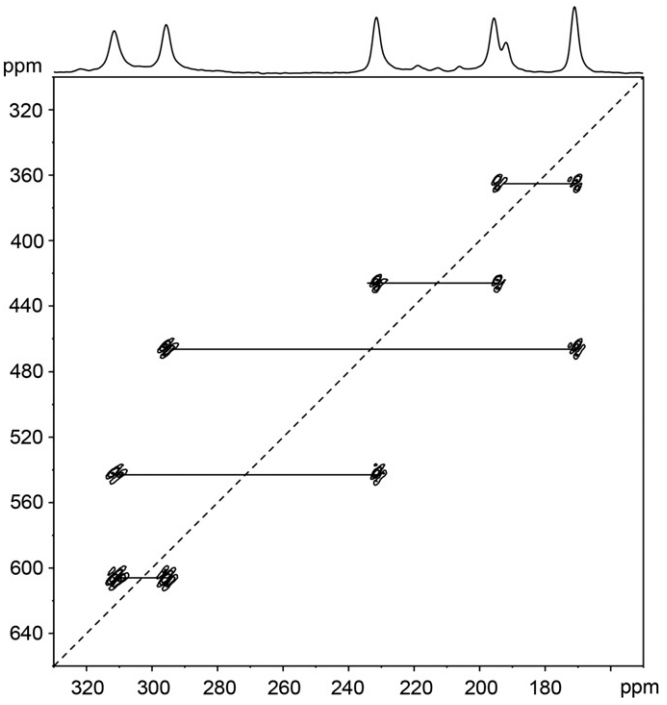

Fig. 3. ^{29}Si 2-D-INADEQUATE MAS-NMR spectrum of $Li_{12}Si_7$. The small observed splittings arise from the antiphase character of the cross-peaks.

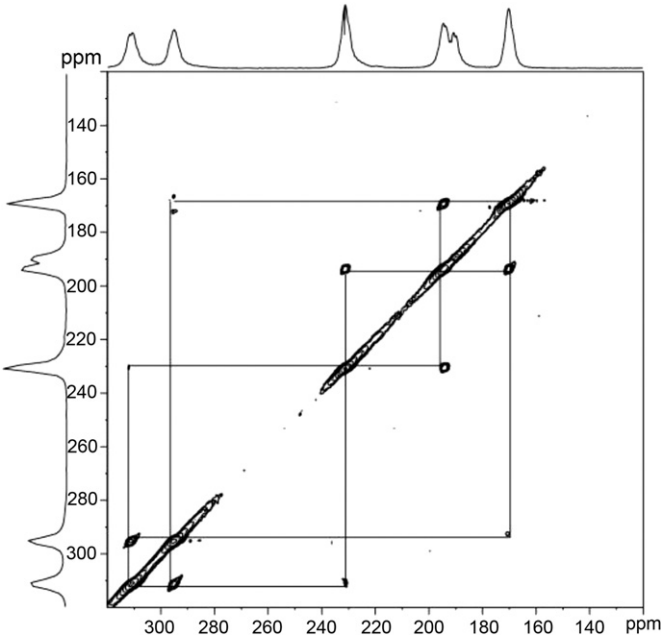

Fig. 4. ^{29}Si 2-D RFDR spectrum of $Li_{12}Si_7$.

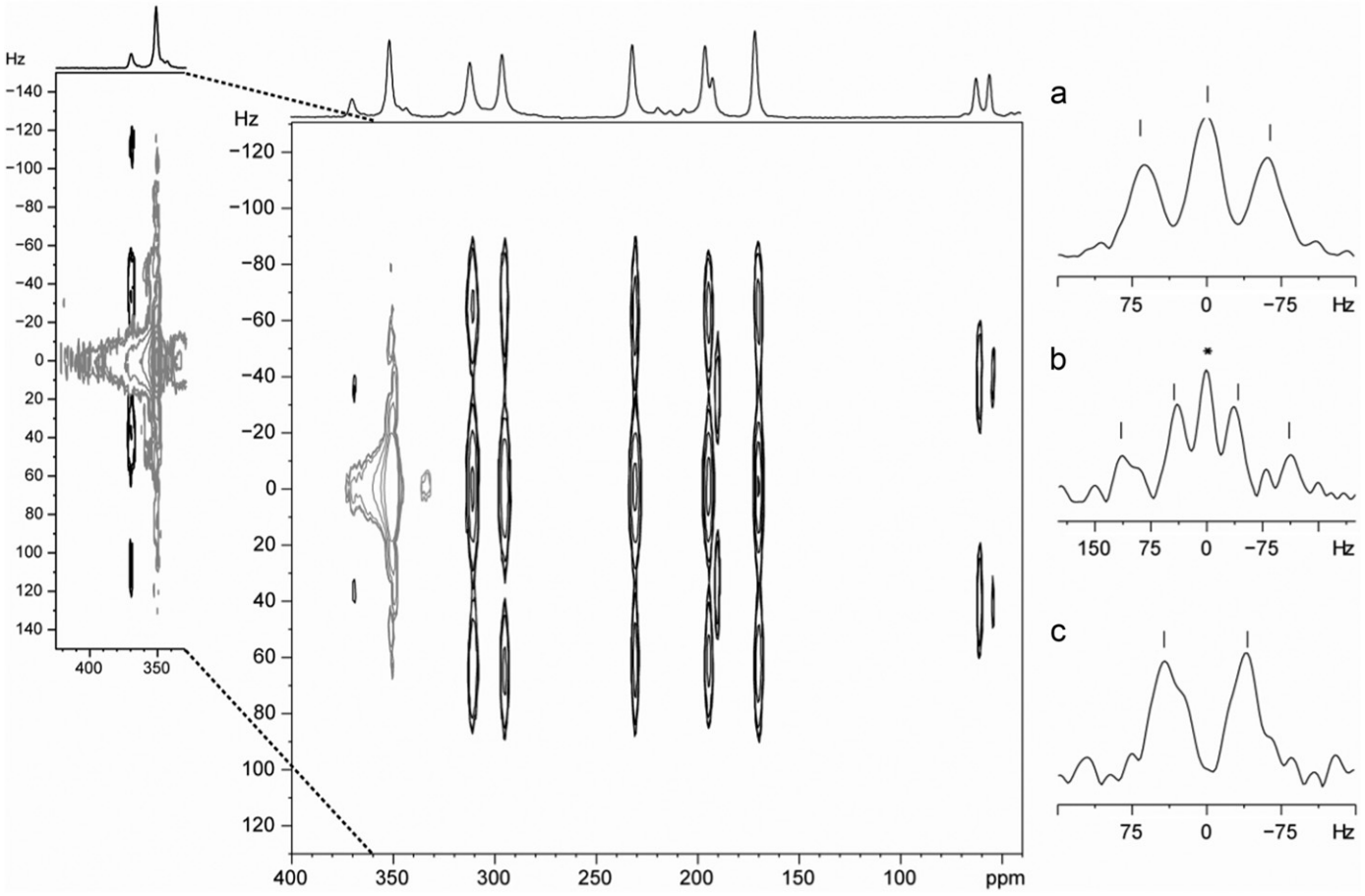

Fig. 5. ^{29}Si 2-D J-resolved MAS-NMR spectrum of $Li_{12}Si_7$. The strong singlet arising from the impurity resonance is displayed in gray color. Individual slices along the F1 dimension, taken at (a) 231.5 ppm (b) 369.5 ppm, and (c) 62.1 ppm, are shown. Peaks belonging to the multiplets are marked by a dash, the overlap of the impurity phase and the quartet is marked by an asterisk. For reasons of clarity, the insert magnifies the region around 369.5 ppm at a lower contour level, showing the quartet structure of the magnetic hyperfine coupling.

Table 1
^{29}Si isotropic chemical shifts, fractional peak areas, spin–spin coupling multiplicities m and ^{1}J coupling constants in $Li_{12}Si_7$.

Si moiety	δ_{iso} (ppm)	I_{tot} (%)	m	^{1}J (Hz)	Si site	
Si_4 (star)	369.5	7	q	74	Si6	
Si_4 (star)	191.8	6	d	82	Si7	
Si_4 (star)	62.1	7	d	82	Si8 or 9	
Si_4 (star)	55.5	6	d	82	Si8 or 9	
					Scen.A	Scen.B
Si_5 (ring)	311.5	12	t	62	Si3	Si4
Si_5 (ring)	295.7	12	t	62	Si2	Si5
Si_5 (ring)	231.5	12	t	62	Si4	Si3
Si_5 (ring)	195.7	14	t	62	Si5	Si1
Si_5 (ring)	171.1	13	t	62	Si1	Si2

3.2. ^{6}Li MAS-NMR and ^{29}Si{^{7}Li} HETCOR NMR

The room temperature ^{6}Li MAS-NMR spectrum of $Li_{12}Si_7$ is shown in Fig. 6. Three distinct resonance lines are observed at 20.3 ppm (8% of the signal area), 15.9 ppm (84% of the signal area) and −17.4 ppm (8% of the signal area), indicating the absence of complete motional averaging on the kHz timescale. As discussed further below on the basis of detailed temperature dependent spectra, the dominant resonance at 15.9 ppm comprises a pool of highly mobile lithium species, whereas the mobilities of the other two lithium species are more restricted. This differential lithium mobility becomes also quite apparent in the ^{29}Si{^{7}Li} HETCOR results at room temperature, obtained on an isotopically enriched material (see Fig. 7). The projection of the 2-D plot in the ^{7}Li dimension reveals a completely different intensity distribution than the ^{6}Li one-pulse spectrum: while in the latter the signal near 15.9 ppm is dominant, its intensity is significantly attenuated in the CP-HETCOR spectrum, where the resonances at 20.3 ppm and −17.4 ppm are greatly emphasized. As ascertained by appropriate control experiments this difference is unrelated to any differences in the spin lock characteristics of the various ^{7}Li species present; as a matter of fact, our results (not shown here) indicate that the ^{7}Li species at 15.9 ppm has the longest rotating frame spin-lattice relaxation time under the conditions used for these CPMAS experiments. Therefore, these intensity variations must be attributed to differences in cross-relaxation efficiencies, reflecting the relative ^{7}Li–^{29}Si dipolar coupling strengths. Thus, our result indicates that the two lithium species reflected by the 20.3 and the −17.4 ppm resonances have significantly lower ionic mobilities in comparison to the majority of the lithium species, which contribute to the motionally averaged signal at 15.9 ppm. Furthermore, the HETCOR spectrum enables a partial assignment of the lithium and the silicon resonances, which can be discussed in relation to the crystallographic distance correlation map presented in Table 2 in matrix form. The −17.4 ppm signal is strongly correlated with all of the five silicon species of the Si_5 rings, but not with the observable terminal ^{29}Si species of the Si_4 star unit at 191.8 ppm. Based on this result (and further

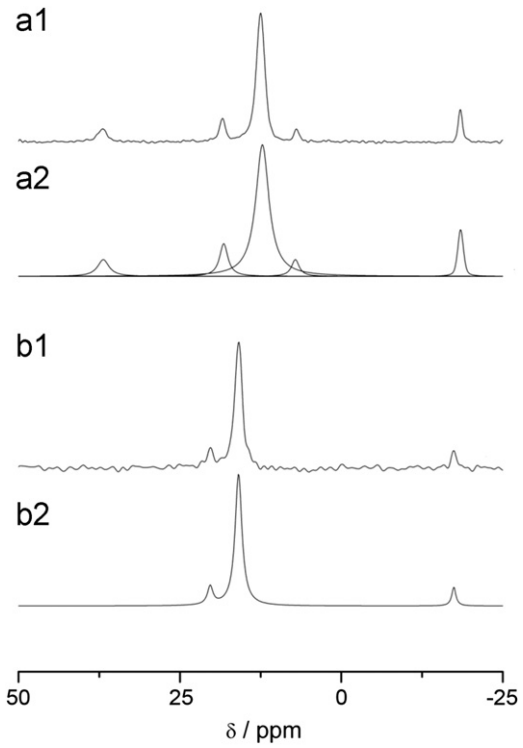

Fig. 6. Room temperature (b) and 200 K (a) ^{6}Li MAS-NMR spectrum of $Li_{12}Si_7$, including the corresponding simulations.

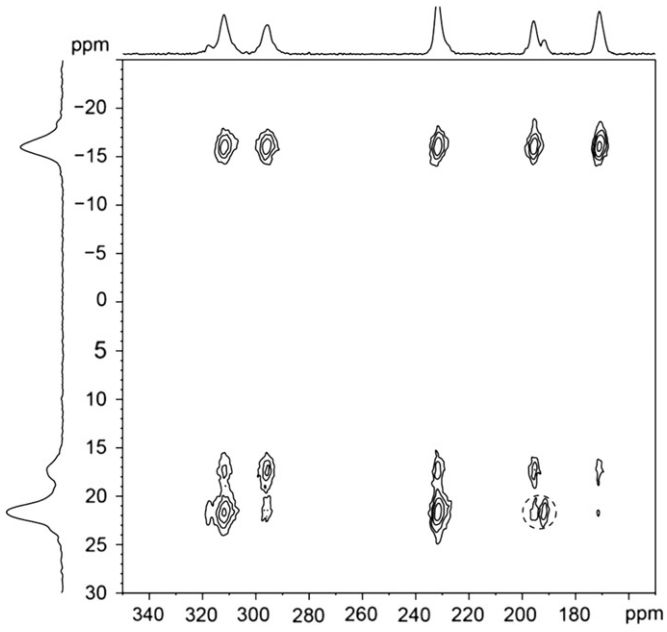

Fig. 7. Room temperature {^{7}Li}^{29}Si HETCOR spectrum of $Li_{12}Si_7$. The cross-peak indicating a suggested correlation between Li3 and Si7 is circled.

arguments presented below), the −17.4 ppm signal can be assigned to the Li6 site. Likewise, the ^{6}Li resonance at 20.3 ppm appears strongly correlated with two silicon species of the Si_5 ring units, however, in this case an additional strong correlation appears with the ^{29}Si NMR signal of the terminal group of the Si_4 star unit. Based on arguments discussed further below this signal can be attributed to the Si7 site. Since none of the other silicon atoms of the Si_4 star can be detected via cross-polarization, the particular lithium species (at 20.3 ppm) close to this silicon must be distant from all the other silicon atoms of the star unit.

Table 2
Li–Si distances (in pm) within the first coordination sphere ($d < 310$ pm) in $Li_{12}Si_7$.

	Si								
Li	**1**	**2**	**3**	**4**	**5**	**6**	**7**	**8**	**9**
1				266	269	281			267
					303				
2		269	262	266	280				
		283			283				
3			269	264			270		
			283	282					
4		270	273	278	270				
					282				
5	268	281			270				278
					280				
6	290	284	289	293	284				
	294	309	299	298	306				
7		293						273	267
8				271		292	278		273
							278		
9			271			284	279	273	
							284		
10		307	263		270			274	
11				266	269	281			267
12	265								299
	265								
13	288					289		281	264
	288								

Comparison of this heteronuclear dipolar coupling profile with Table 2 suggests an assignment of the 20.3 ppm resonance to Li3. Based on this assignment, the ^{29}Si NMR signals at 311.5 and 231.5 ppm belong to the Si3 and Si4 sites (or vice versa), which have the closest distances to the Li3 species. This assignment is also consistent with the INADEQUATE and RFDR results, which reveal strong dipolar correlations between these two silicon species. Based on the homonuclear connectivities detected by these dipolar experiments we can propose two alternate assignment scenarios for the silicon atoms of the Si_5 ring units (see Table 1).

3.3. *Variable temperature high-resolution ^{6}Li NMR*

The ^{6}Li spectrum recorded at 200 K (Fig. 8) shows five resolved resonances: a dominant line at 12.7 ppm, accounting for about 70% of the total signal area and four distinct peaks at 37.1 (9%), 18.7 (8%), 7.1 (5%), and −18.3 ppm (8%). The fractional areas of these signals (with the exception of the 7.1 ppm peak) are close to 8.3% as expected for each crystallographically distinct lithium site that would be individually resolved in the spectrum. The area of the 7.1 ppm peak suggests that this peak has to be attributed to one of the two lithium species (Li12 or Li13) that have only half of the Wyckoff multiplicity of the other sites (4 instead of 8). Correspondingly the other lithium site with Wyckoff multiplicity of 4 must contribute to the majority peak at 12.7 ppm.

The chemical shifts of the lithium ions in $Li_{12}Si_7$ are expected to be influenced by both Knight shift contributions arising from conduction electron density localized at the lithium sites as well as the diamagnetic anisotropy arising from electrons in π orbitals associated with the Si_5 ring and the Si_4 star moieties, both of which have planar geometries. In approaching resonance assignments, previous electronic structure calculations [8,16–19] as well as the proximity and orientation of the various lithium sites with respect to these Si structural moieties must be considered. Table 2 indicates that most lithium species have closest distances to silicon atoms belonging to both the Si_5 rings and the Si_4 stars. Nevertheless, for most of the lithium positions the proximity to one of the units dominates. Because of the strong π-electron

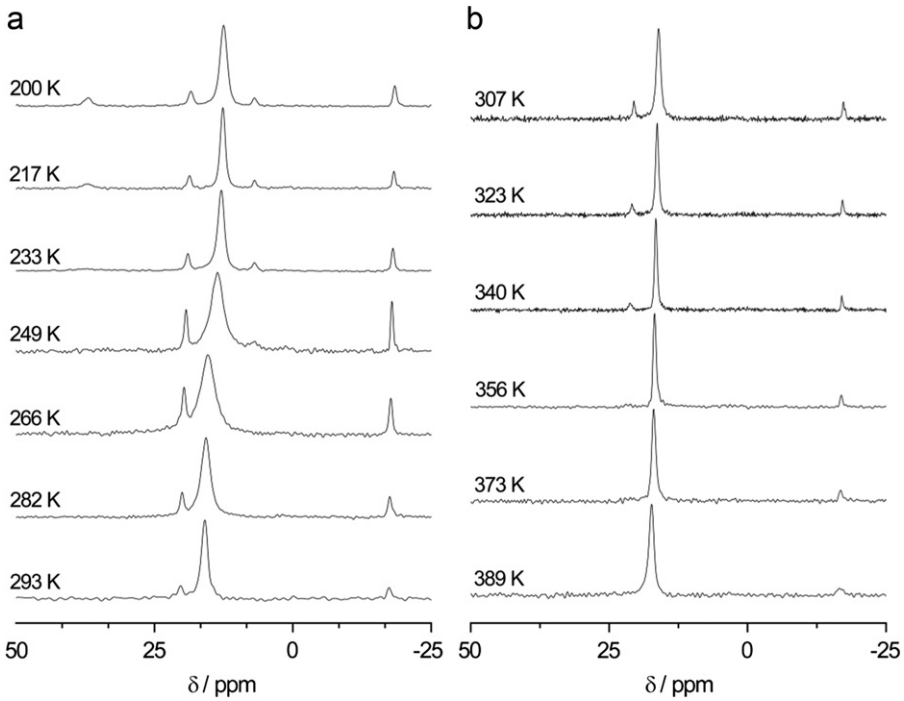

Fig. 8. Variable temperature ^{6}Li MAS-NMR spectra of $Li_{12}Si_7$: (a) high temperature MAS (b) room temperature and below.

contribution present in the planar cyclic Si_5 units, the bonding in the latter has been described as "aromatic-like" [8]. Consequently, these units are expected to have a particularly large diamagnetic anisotropy, sometimes referred to as "ring current effect". Based on these considerations, we can assign the distinct low-frequency resonance to the Li site Li6 positioned directly above the five-membered ring structural element. The strong diamagnetic displacement is comparable to that in lithium cyclopentadienide (LiCp), where the lithium ions situated above the cyclopentadienyl rings give a resonance shift of −9 ppm [26]. Furthermore, the resonance at 37.1 ppm with its strongest Knight shift contribution is likely to reflect a lithium ion closely interacting with the Si_4 star unit. Assignments of the other resonances to specific lithium species are not possible at this stage, as the dominant resonance most likely still represents numerous motionally averaged lithium sites. Fig. 8 shows detailed temperature dependent spectra. Most significantly, the high-frequency resonance near 37.1 ppm broadens above 200 K and disappears at higher temperature. This effect is accompanied by significant broadening of the dominant resonance and a gradual shift from 12.2 towards 16.5 ppm indicating signal coalescence due to dynamic exchange. Above 250 K, the lithium species belonging to the 7.1 ppm resonances are implicated in this exchange as well, so that at and above room temperature 84% of the lithium species now belong to a single pool of lithium ions with jump rates significantly higher than 1 kHz. Towards increasing temperatures two distinct lithium ions with lower mobilities still persist in the spectrum. One of them is the Li6 species, observed near −17 ppm (8% of the signal area), indicating that this lithium species does not take part in the motional averaging process up to temperatures of 360 K. Signal coalescence effects for this peak finally become noticeable at 389 K, the highest temperature investigated. Incomplete motional averaging at room temperature is further indicated by a signal near 20.3 ppm (8%), tentatively assigned to the Li3 site. According to Fig. 8, however, this lithium species appears to have a somewhat higher mobility than Li6, as chemical exchange effects and signal coalescence are being observed already above 340 K. The thermal activation of ionic motion involving the Li3 and Li6 sites may well be related to the two distinct relaxation mechanisms observed by Kuhn et al. in their rotating-frame spin lattice relaxation experiments [15].

Fig. 9 shows corresponding ^{6}Li MAS-NMR results for $Li_{12}Ge_7$, which are completely analogous. At low temperatures multiple peaks are observed as for $Li_{12}Si_7$, at 46.3 ppm (7%), 27.0 ppm (13%), 17.2 ppm (50%), 12.3 ppm (7%), and 8.5 ppm (4%). Some of these resonances are rather broad, indicating that at the temperature of the measurement (200 K) chemical exchange processes due to lithium motion on the MAS-NMR timescale are not yet suppressed; unfortunately lower temperatures were not attainable with the equipment used. Based on its low intensity, the peak at 8.5 ppm must be assigned to one of the two lithium sites with lower Wyckoff multiplicity (Li12 or Li13). Finally, the low-frequency resonance attributable to the lithium species above the ring is observed at −17.4 ppm (11%). The slightly smaller diamagnetic effect in the Ge compound compared to the Si compound might be explained by the larger size of the Ge compared to the Si atoms, leading to decreasing overlap between the p-orbitals that form the π-system and larger Ge–Li distances (3.00–3.06 Å) as compared to $Li_{12}Si_7$ (2.89–3.06 Å). At room temperature, these lithium species are still being observed as a distinct resonance at −16.4 ppm (8%), again indicating that this lithium species does not participate in the motional averaging process. Altogether, these results indicate that both the electronic structures and the lithium ionic mobility profiles of both compounds are completely analogous to each other.

3.4. *Variable temperature static ^{7}Li NMR*

Variable temperature static ^{7}Li NMR spectra and the corresponding plots of the full widths at half height are shown in Figs. 10 and 11. The data illustrate the high mobility of the lithium ions, which has been recently characterized in detail by rotating frame relaxation time studies [15]. The activation energy of lithium ionic motion can be estimated from the variable

temperature spectra, using the expression of Waugh and Fedin [27], E_a [eV] $\approx 1.617 \times 10^{-3} T_{on}$ [K], where T_{on} stands for the onset temperature of the motional narrowing, The activation energies of 0.19 eV in $Li_{12}Si_7$ is in good agreement with that published previously by Kuhn et al. on this compound [15]. Analogous results, with an estimated activation energy of 0.2 eV are obtained on $Li_{12}Ge_7$ (Fig. 11), revealing much faster lithium dynamics than those previously observed in ternary lithium tetrelides [28,29].

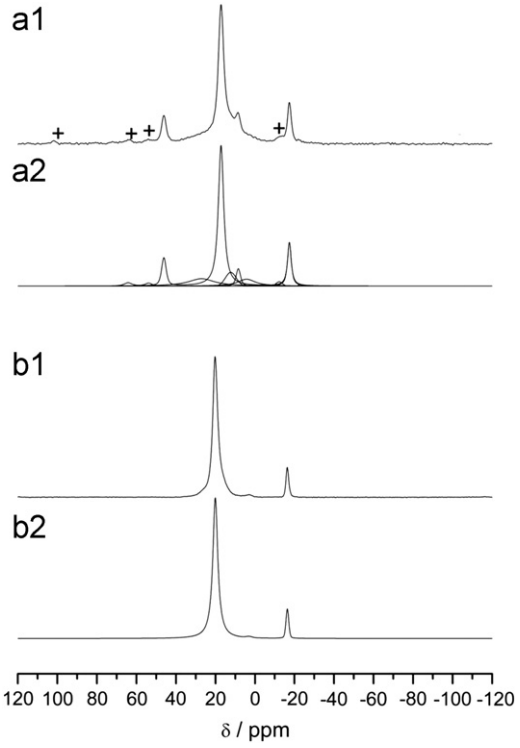

Fig. 9. Room temperature (b) and 200 K (a) ^{6}Li MAS-NMR spectrum of $Li_{12}Ge_7$, including the corresponding simulations. Impurity resonances (less than 2%) are indicated.

4. Discussion and conclusions

In summary, the results of the present study clearly illustrate the power and potential of variable temperature magic-angle spinning NMR spectroscopy to provide detailed structural information about the local silicon and lithium ion environments in $Li_{12}Si_7$ and $Li_{12}Ge_7$. The ^{29}Si MAS-NMR spectra, aided by J-resolved spectroscopy, are well suited to differentiate between the individual structural elements within the silicon framework; further detailed connectivity information is available on the basis of 2-D INADEQUATE and RFDR spectra, leading to two tentative assignment scenarios summarized in Table 1. While the wide ^{29}Si chemical shift range observed with these compounds indicates the great sensitivity of this parameter to the local electronic environments on these sites, a detailed consideration of the crystal structure indicates no straightforward structural correlations with Si–Si bond lengths or Si–Si–Si bond angles. Still, it is worth pointing out, that assignment scenario B leads to a monotonic ordering of the chemical shifts with the average Si–Si bond lengths. Thus, according to this scenario, Si4, which has the smallest average bond length (236.0 pm), is found at the highest chemical shift, and Si2, which has the largest average bond length (237.5 pm) is found at the lowest chemical shift. Intermediate chemical shifts are found for the other three silicon atoms, having their average bond lengths of 236.8 (Si5), 236.8 (Si3), and 236.9 pm (Si1). While no such ordering is found for scenario A, the fact that the correlation peak between Li3 and the resonance at 170 ppm has the lowest intensity could speak in favor of that scenario. It is further worth noting that the ordering of the

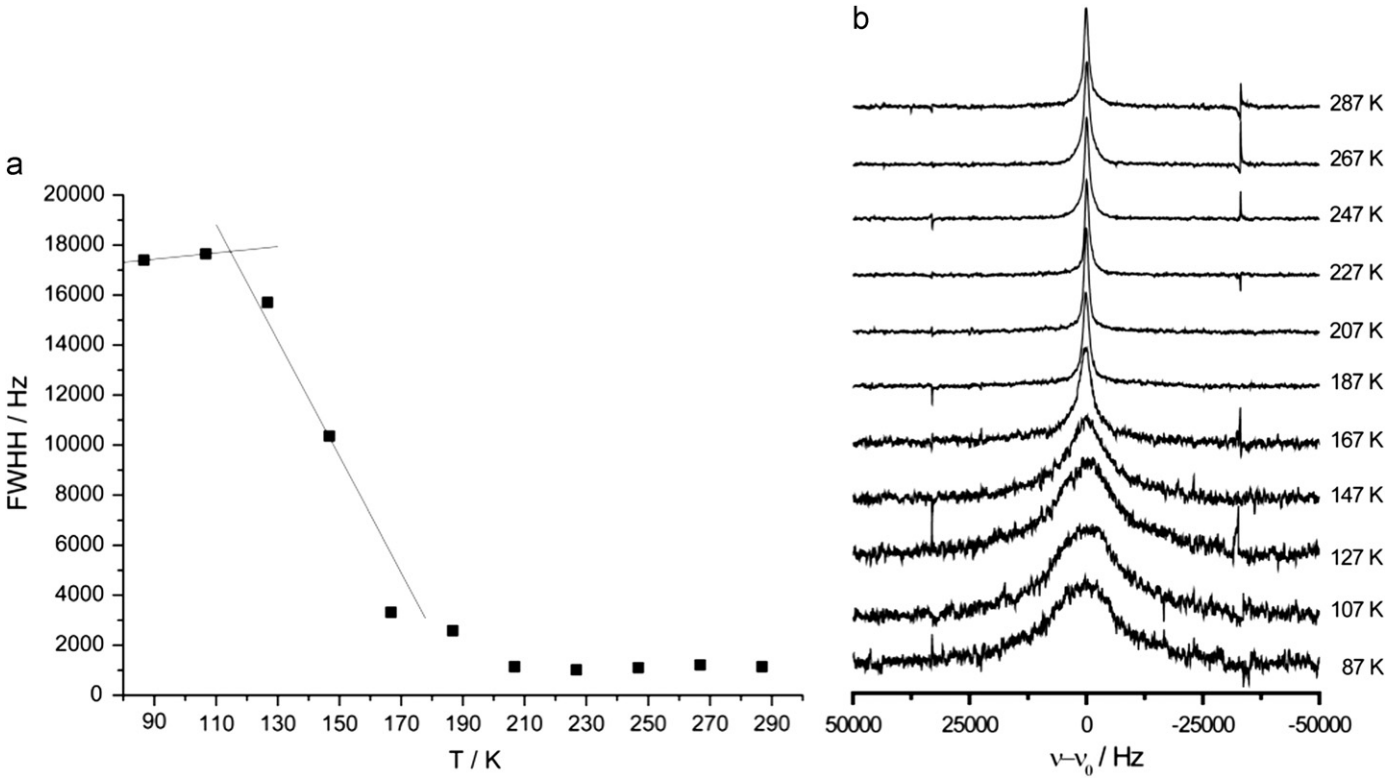

Fig. 10. Variable temperature static ^{7}Li NMR of $Li_{12}Si_7$. (a) temperature dependence of the full width at half maximum, (b) temperature dependent lineshapes.

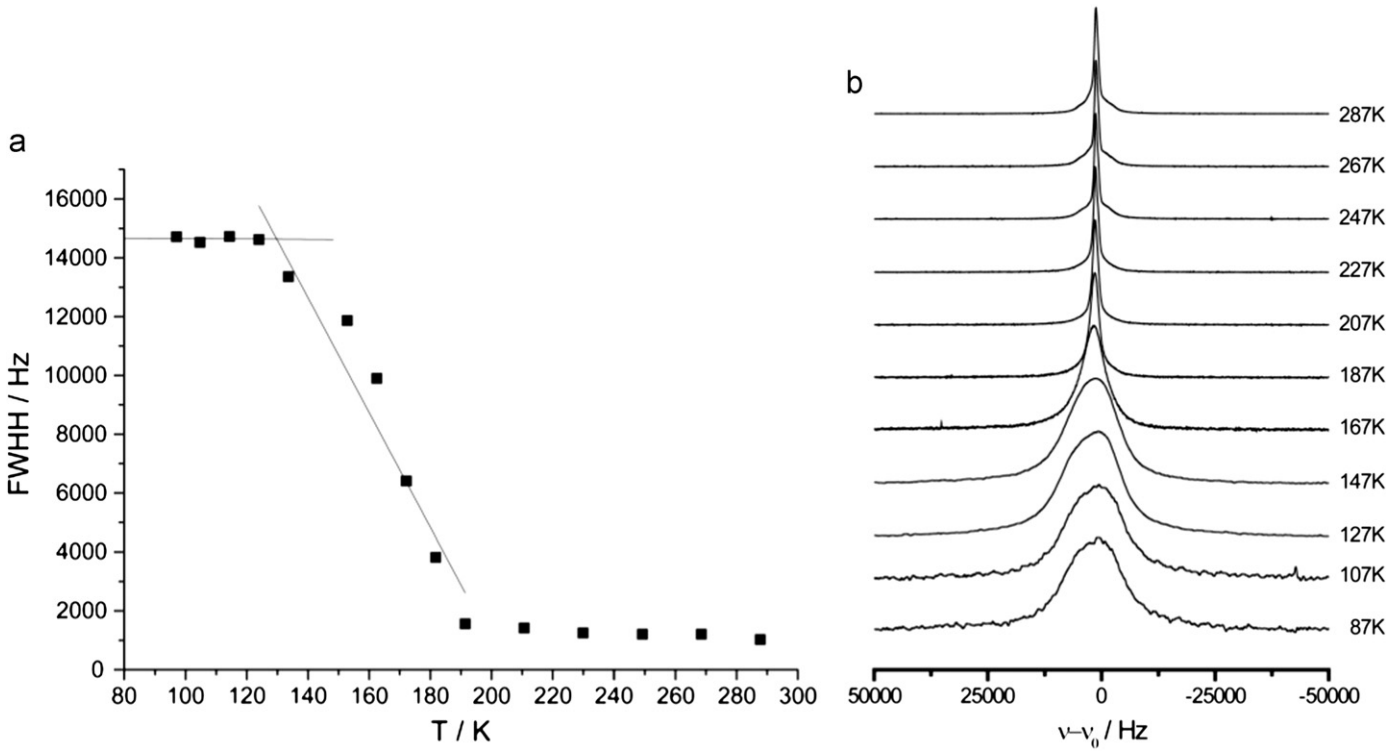

Fig. 11. Variable temperature static ^{7}Li NMR of $Li_{12}Ge_7$. (a) temperature dependence of the full width at half maximum, (b) temperature dependent lineshapes.

chemical shifts of the terminal Si atoms of the Si_4 star unit can be understood analogously. Si7 with its much shorter average Si–Si bond length (236.3 pm) appears at a higher chemical shifts than Si8 and Si9, whose Si–Si bonds are significantly longer (237.9 and 239.1 pm, respectively). Additional support for scenario B could in principle be furnished by a low-temperature HETCOR experiment, in which the chemical shift of the Si1 site would be identified based on a strong heteronuclear correlation with the 7.1 ppm resonance assigned to either Li12 or Li13 (see below). We attempted this experiment, however, unfortunately, found it to be sabotaged by strong overlapping spinning sidebands arising from the $^{7}Li \pm 1/2 \leftrightarrow \pm 3/2$ Zeeman transitions, which are broadened by the anisotropy of the nuclear electric quadrupolar interactions. While it is possible to suppress these sidebands by off-angle spinning, misadjusting the magic angle for this purpose also degraded the resolution in the ^{29}Si dimension. The best possible way to address this problem would be a ^{6}Li/^{29}Si HETCOR experiment on a doubly isotopically enriched sample. While such experiments are very demanding owing to the small frequency difference between the two nuclei involved, they are under consideration for future studies.

Regardless of the assignment issue, the results of the present study indicate the need for more sophisticated theoretical approaches for predicting Knight shifts and chemical shifts in intermetallic compounds. With regard to the bonding state of the lithium ions various calculations with different degrees of sophistication and quantitative evaluation have been published previously [8,16–19], indicating significant variations in the amount of charge situated on the lithium. Specifically, the Li6 species situated directly above the five-membered Si_5 and Ge_5 rings (labeled Li8 in Ref. [19]) stand out in terms of their peculiar bonding situation and do not participate in the fast motional averaging processes; likewise Li3 is significantly slower than most (84%) of the other lithium species. The differential lithium mobilities have been monitored by detailed variable temperature ^{6}Li MAS-NMR studies, indicating exchange broadening and coalescence phenomena for the less-mobile lithium ions on the MAS-NMR timescale. For the majority of the highly mobile lithium ions, activation energies near 0.2 eV have been estimated from variable temperature ^{7}Li static NMR lineshape analyses.

Acknowledgments

This work was supported by the DFG research Grant Ec168/9-1 within the Schwerpunktprogramm "Lithium High Performance Batteries." S.D. thanks the Fonds der Chemischen Industrie for a personal fellowship. We also thank Dr. Alice Cattaneo and Dipl.-Chem. Thomas Wiegand for helpful discussions.

References

[1] R. Nesper, Prog. Solid State Chem. 20 (1990) 1.
[2] R. Nesper, H.G. von Schnering, J. Solid State Chem. 70 (1987) 48.
[3] W. Klemm, M. Struck, Z. Anorg. Allg. Chem. 278 (1955) 117.
[4] B.A. Boukamp, G.C. Lesh, R.A. Huggins, J. Electrochem. Soc. 128 (1981) 725.
[5] R. Nesper, H.G. von Schnering, J. Curda, Chem. Ber. 119 (1986) 3576.
[6] U. Frank, W. Müller, H. Schäfer, Z. Naturforsch. B 30 (1975) 10.
[7] H.G. von Schnering, R. Nesper, K.F. Tebbe, J. Curda, Z. Metallkd. 77 (1980) 357.
[8] H.G. von Schnering, R. Nesper, J. Curda, K.F. Tebbe, Angew. Chem. 92 (1980) 1070.
[9] P. Limthongkul, Y.I. Jang, N.J. Dudney, Y.M. Chiang, J. Power Sources 119–121 (2003) 604.
[10] B. Key, R. Bhattacharyya, M. Morcrette, M.V. Sceneac, J.M. Tarascon, C.P. Grey, J. Am. Chem. Soc. 131 (2009) 9239.
[11] B. Key, R.M. Morcrette, J.M. Tarascon, C.P. Grey, J. Am. Chem. Soc. 133 (2011) 503.
[12] H. Trill, C. Tao, S. Passerini, M. Winter, H. Eckert, J. Solid State Electrochem. 15 (2011) 349.
[13] M.N. Obrovac, L. Christensen, Electrochem. Solid-State Lett. 7 (2004) A93.
[14] T.D. Hatchard, J.R. Dahn, J. Electrochem. Soc. 131 (2004) A838.
[15] A. Kuhn, P. Sreeraj, R. Pöttgen, H.-D. Wiemhöfer, M. Wilkening, P. Heitjans, J. Am. Chem. Soc. 133 (2011) 11018.
[16] M.C. Böhm, R. Ramirez, R. Nesper, H.G. von Schnering, Phys. Rev. B 30 (1984) 4870.
[17] J.F. Liebmann, J.S. Vincent, Angew. Chem. 94 (1982) 649.
[18] H. van Leuken, G.A. de Wijs, W. van der Lugt, R.A. de Groot, Phys. Rev. B 53 (1996) 10599.

[19] V.L. Chevrier, J.W. Zwanziger, J.R. Dahn, J. Alloys Compd. 496 (2010) 25.
[20] A. Bielecki, D.P. Burum, J. Magn. Reson. A 116 (1995) 215.
[21] T. Takahashi, H. Kawashima, H. Sugisawa, T. Baba, Solid State Nucl. Magn. Reson. 15 (1999) 119.
[22] D. Massiot, F. Fayon, M. Capron, I. King, S. Le Calvé, B. Alonso, J.O. Durand, B. Bujoli, Z. Gan, G. Hoatson, Magn. Reson. Chem. 40 (2002) 70.
[23] M. Bourdonneau, B. Ancian, J. Magn. Reson. 132 (1998) 316.
[24] A.E. Bennett, C.M. Rienstra, J.M. Griffiths, W. Zhen, P.T. Lansbury, R.G. Griffin, J. Chem. Phys. 108 (1998) 9463.
[25] P.K. Jenkner, A. Spielberger, M. Eibl, E. Hengge, Spectrochim. Acta 49A (1993) 161.
[26] D. Johnels, A. Boman, U. Edlund, Magn. Reson. Chem. 36 (S1) (1998) 151.
[27] J. Waugh, I. Fedin, Sov. Phys. Solid State 4 (1963) 1633.
[28] Z. Wu, B.D. Mosel, H. Eckert, R.-D. Hoffmann, R. Pöttgen, Chem. Eur. J. 10 (2004) 1558.
[29] Z. Wu, R.-D. Hoffmann, D. Johrendt, B.D. Mosel, H. Eckert, R. Pöttgen, J. Mater. Chem. 13 (2003) 2561.